Various pathogen-laden aerosol deposition in the realistic human airway during inhalation

Danting Luo [1], *Xiaohong Zheng* [1,2], and *Hua Qian* [1,2*]

[1] School of Energy and Environment, Southeast University, Nanjing, China
[2] BEEE, Southeast University, Nanjing, China

Abstract. Studying the deposition of different pathogens with various sizes and shapes is vital for understanding various respiratory infectious diseases. Few studies focus on the deposition of pathogen-laden aerosol during inhalation, especially for different respiratory infectious pathogens. This paper studied the depositions of H3N2, SAR-CoV-2, Ebola virus, Escherichia coli, and different sizes of droplets in the realistic human respiratory airway during inhalation. And results show that large droplets are mainly deposited in the upper respiratory tract, while most of the small particles, especially viruses, will transmit to somewhere further than bronchi-G7 and be deposited into the deep lobes of the lungs. Over 90% of single virus particles will inhale into lobes. The deposition efficiency of pathogens in the right lobes is significantly higher than that in the left, and this phenomenon is more obvious in the superior lobes, which may also explain why lung carcinomas are more likely to develop in the right lung. Compared with other viruses, SARS-CoV-2 is more inhaled into the right superior lobe, which should be paid attention to. This paper may help learn about various respiratory infectious diseases and provide references for treatment methods and drug delivery locations.

1 Introduction

Respiratory infectious disease constantly threatens people's lives and health. Seasonal influenza virus, which is major caused by the influenza A/H3N2[1], results in about 3 to 5 million cases of severe illness and 0.29 to 0.65 million deaths annually; The outbreak of Ebola viruses during 2013–2016 in west African causes more than 28 000 confirmed cases and 11 000 deaths[2]; Severe Acute Respiratory Syndrome Coronavirus 2 (SARS-CoV-2) infects more than 427 million people worldwide, including over 5.9 million deaths by February 2022. Besides viruses, potentially pathogenic microorganisms[3] are also recognized as agents to cause respiratory infections, such as Escherichia coli[4], Legionella[5]. Inhaling pathogen-laden aerosol is considered as the main route to infect. After inhaling, pathogen-laden aerosols will deposit and replicate in the respiratory tract. Deposition conditions of pathogen-laden aerosols determine patient disease progression and reveal the location where producing the exhaled pathogen-laden aerosol[6].

The deposition is affected by particle shapes and sizes[7,8]. The drag force, which affects particle tracking and deposition, is quite different between non-spherical shape particles and spherical shape particles[9]. For different sizes in the same shape, ultrafine particles have been proved can reach the most distal lung regions[10], and large particles always deposit in the upper airways[11]. Although the deposition of PM 2.5, nanoparticles, droplets has been preliminarily studied, few studies focus on the deposition of various respiratory infectious pathogen-laden aerosols. Moreover, the filamentous shape of the virus is verified to have an infectivity advantage under any cell-entry pressure than spherical shape[12], which implies the importance of understanding the deposition of pathogen-laden aerosols, especially in various shapes.

Simplified lung geometries are widely applied for investigating particle deposition due to the delicate and complex nature of the human airways, especially Horsefield's model[13] and Weibel's model[14]. However, these models simplify too much detail and hard to obtain more realistic deposition results. In recent years, the realistic human airway model has been well developed by CT scans and MRI measurements, making it possible to obtain a physiologically realistic airway geometry. Some models only focus on the human upper airway, but small particles like viruses deposit on the lower airway, which requires the lower airway model. Beyond the 7th or 9th generation, the bifurcation model is hardly provided only based on the inadequate clarity of the scanned images, so four-dimensional CT[15,16], 3-D U-Net[17], and digital topologic[18] are used to reconstruct more distal bifurcation. Compared with the bifurcation structure of higher generation, the deposition in different lobes seems more worthy to study since those small pathogen-laden aerosols always rush deep into the lobes. Lung carcinomas, including primary small cell carcinoma and non-small cell carcinoma, are more likely to develop in the right than left lung[19-21], which may be affected by non-uniformity of lobar

* Corresponding author: qianh@seu.edu.cn

deposition[22]. The deposition of pathogen-laden aerosols may also present this condition which needs to be approved in a realistic human airway and five-lobe lung model.

The numerical simulation is the best choice for studying the deposition of respiratory infectious pathogen-laden aerosols since in vivo measurement inside the lungs is impossible and in vitro measurement of real pathogens has exposure risk. This paper studied the depositions of various respiratory infectious pathogens and different sizes of droplets in the realistic human respiratory tract calculated by CFD. It may help to learn more about various respiratory infectious diseases and provide references to give treatment methods and drug delivery locations.

2 Methods

2.1 Realistic human respiratory tract and lobes model

The realistic human respiratory tract and lobes model was reconstructed based on a healthy adult's CT image with 1 mm distance between slices. It includes an upper respiratory tract (nasal and oral cavities, pharynx, and larynx), and a lower respiratory tract (extending from the trachea to bronchi-G7), as shown in Figure 1.

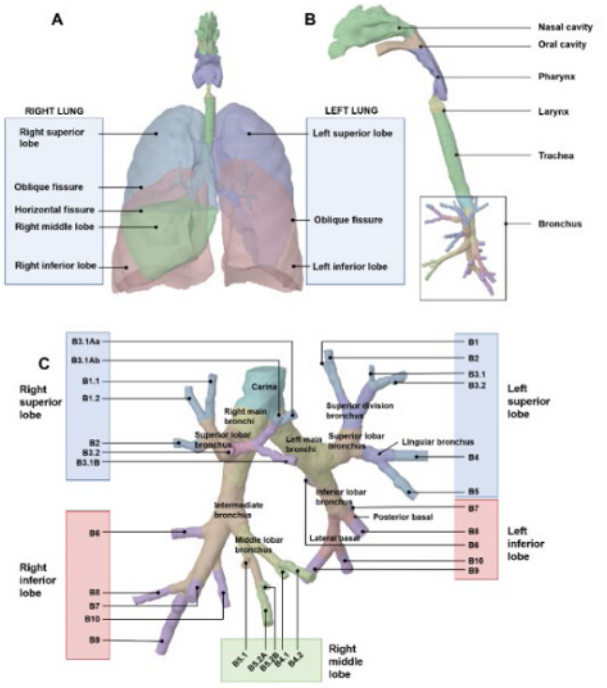

Figure 1. Realistic model of the human respiratory tract and lobes. (A) lobes and fissures; (B) respiratory tract; (C) details of the bronchus.

2.2 Flow field

We employ the finite volume method to solve the governing equations for the flow. RANS low-Re k-ω-SST is used as the turbulence model since it is best to capture the mean flow characteristics[23]. The SIMPLE coupling scheme, hybrid initialization, and pressure-based solver are used. The second-order upwind technique is utilized for momentum equations.

2.3 Particle tracking

We employed a Lagrangian particle-tracking approach and the one-way coupling approach to model the aerosol transport and deposition in the airways. The dilute bioaerosol (discrete phase) is considered a dilute suspension with non-rotating particles, so the inter-particle interactions (collide with each other and aggregate) are neglected. Affected by mucus in the airway, particles will be trapped immediately, particle-wall interaction is also neglected. The deposition fraction (DF) is defined as:

$$DF\ (\%) = \frac{\text{The number of particles deposited on a section of the walls}}{\text{The total number of particles entering that section of the wall}} \times 100, \quad (1)$$

Due to the large particle-to-fluid density ratios for aerosol particles in the air and the low-Reynolds number flows, the Saffman lift, pressure gradient, added mass, and Basset forces are also considered insignificant. Equations of motion for bioaerosol particles is given by:

$$\frac{du_p}{dt} = g\frac{\rho_p - \rho_f}{\rho_p} + \frac{3\rho_f}{4\rho_p d_p}\frac{C_D}{C_c}(u_f - u_p)\left|u_f - u_p\right| \quad ,(2)$$

where t is the time and g is gravity vector. u and ρ denote the velocity and density, while superscripts p and f refer to particles and fluid, respectively. C_D and Cc are the drag coefficient and the Cunningham correction to drag force. The cunningham correction is considered in those particles whose diameter is lower than 1um.

The diameters of various pathogens and different size droplets are shown in Table 1. Since the breathing process is fast (breathing rate at the mouth Q=30L/min), mass transfer effects on droplet size are not taken into account. And the particle density was set to $\rho_p = 998.2$ kg/m3.

Table 1. The diameters of various pathogens and different size droplets.

Type	Name	Shape	Equivalent diameter	Degree of sphericity
Virus	H3N2 [24,25]	Filamentous	0.223 um	0.64
		Spherical	0.12 um	1
	SAR-CoV-2[26]	Spherical	0.08-0.4 um	1
	Ebola virus[27]	Filamentous	0.224 um	0.63
Potentially pathogenic Microorganisms	Escherichia coli[4]	Filamentous	1.22 um	0.59
Droplets		Spherical	1 um	1
			2.5 um	1
			5 um	1
			50 um	1
			100 um	1

2.4 Model validations

The unstructured grid of the respiratory tract model is constructed with tetrahedral cells. Ten layers of prism elements are added to the boundaries of the pharynx, larynx, and trachea, while six layers are added to other parts. We selected a computing mesh with approximately 17.6 million elements among 7.2 million, 9.0 million, 17.6 million, and 21.8 million elements. The

maximum y+ of the airway is below 1.0, while the average y+ is 0.29.

We compared the deposition efficiencies of our results with previously validated research[28-31] to evaluate the validity of the current simulation. Stokes numbers (Stk) are calculated using the airway's diameter and bulk velocity in a particular bifurcation. The deposition efficiencies against various stokes numbers (Stk) are drawn in Figure 2. As can be seen, our results fall within the scatter of the experimental data.

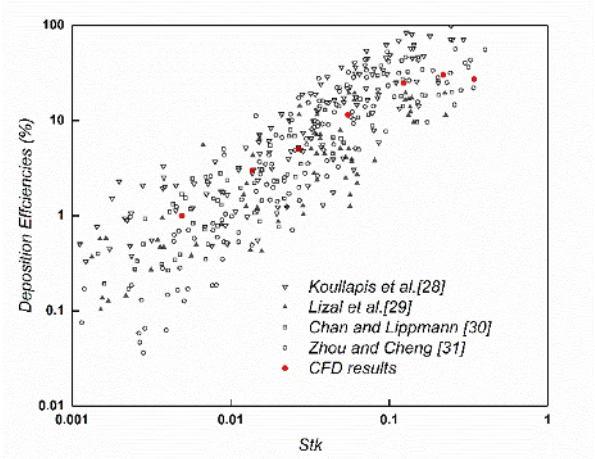

Figure 2. Comparison of the CFD-predicted deposition efficiencies with previously published experimental data.

3 Results and discussions

3.1 The total deposition efficiencies of pathogens and droplets in airway

Large droplets are mainly deposited in the upper respiratory tract, while most of the small particles, especially viruses, will transmit to somewhere further than bronchi-G7 and be deposited into the deep lobes of the lungs, as shown in Figure 3. Indeed, only 12.40% of SARS-CoV-2 and 13.34% of Ebola will deposit before the deep lobes, while the average DF_{airway} of the H3N2 virus for filamentous and spherical shapes is ~11.55%. DF_{airway} of Escherichia coli (~14.99%) is similar with 1 um droplets (~14.54%).

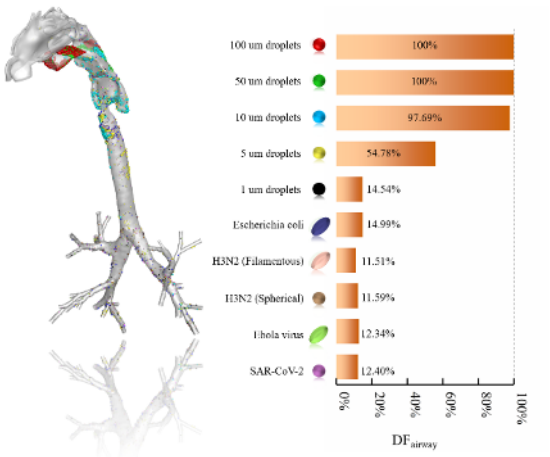

Figure 3. The total deposition efficiencies of pathogens and droplets in airway. The DF_{airway} denotes the total deposition efficiency in the airway, including the upper respiratory tract and part of the lower respiratory tract (extending from the trachea to bronchi-G7).

3.2 The deposition efficiencies of pathogens and droplets in each part

Over 90% (90.74%±0.46%) of single virus particles will inhale into lobes, as shown in Figure 4. The deposition efficiency of pathogens in the right lobes is significantly higher than in the left, and this phenomenon is more obvious in the superior lobes, which may also explain why lung carcinomas are more likely to develop in the right lung. The larynx has gathered many droplets of 5-10um since it is narrow, although the area is small. A few small particles are still transported in the nasal cavity when inhaling through the mouth. 10 um droplets prefer to deposit in the pharynx (~56.93%), followed by the main airway (~22.65%), while 5 um droplets mainly gathered in the larynx and main airway. Compared with other viruses, SARS-CoV-2 is inhaled more into the right superior lobe, which should be paid attention to.

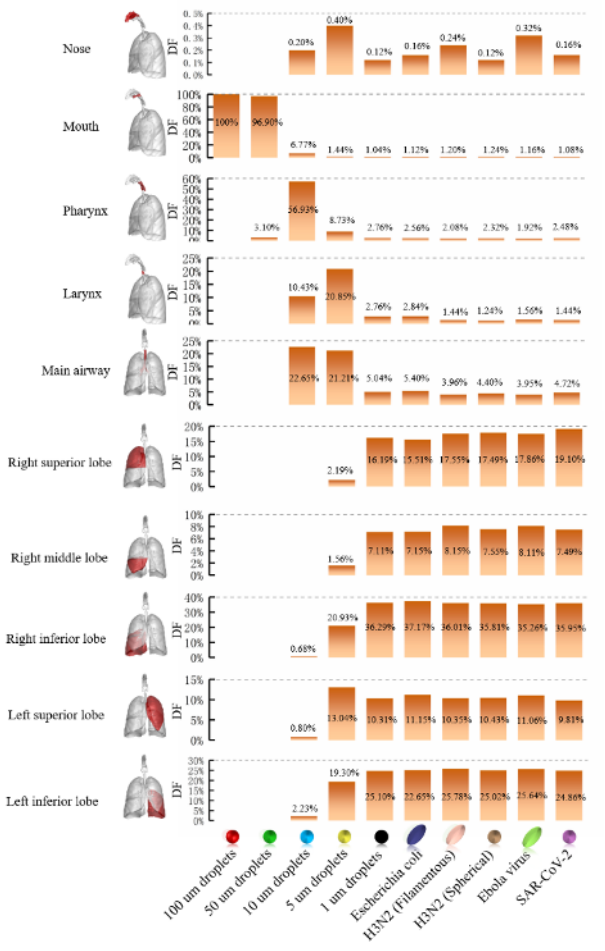

Figure 4. The deposition efficiencies of pathogens and droplets in each part.

4 Conclusions

This paper studied the depositions of various respiratory infectious pathogens and different sizes of droplets in

the realistic human respiratory tract. It shows that large droplets are mainly deposited in the upper respiratory tract, while most of the small particles, especially viruses, will transmit to somewhere further than bronchi-G7 and be deposited into the deep lobes of the lungs. Over 90% of single virus particles will inhale into lobes. The deposition efficiency of pathogens in the right lobes is significantly higher than that in the left, and this phenomenon is more obvious in the superior lobes, which may also explain why lung carcinomas are more likely to develop in the right lung. Compared with other viruses, SARS-CoV-2 is inhaled more into the right superior lobe, which should be paid attention to. It may help to learn more about various respiratory infectious diseases and provide references to give treatment methods and drug delivery locations.

References

1. WHO. Influenza (Seasonal). (2018)
2. T. Garske, A. Cori, A. Ariyarajah, et al. Philos T R Soc B. **372** 1721 (2017)
3. Z. Matkovic, M. Miravitlles. Resp Med. **107**, 1 (2013)
4. T. Kenzaka, A. Ishidoshiro, K. Tani, M. Nasu. Lett Appl Microbiol. **49**, 6, (2009)
5. S. Perinel, V. Forest, M. Landraud, et al. Int J Hyg Envir Heal. **221**, 2, (2018)
6. H. Yu, H. L. Yen, Y. Li. J Aerosol Sci. **142**, (2020)
7. Carvalho TC, Peters JI, Williams RO. Int J Pharmaceut. **406**, (2011)
8. L. Jia, L. Zhang. Acta Scientiarum Naturalium Universitatis Nankaiensis. **52,** 6, (2019)
9. G. Bagheri, C. Bonadonna. Powder Technol. **301**, (2016)
10. H. S. Kwon, M. H. Ryu, C. Carlsten. Exp Mol Med. **52**, 3, (2020)
11. L. P. Nguyen, N. D. Khoa, K. Ito. Indoor Built Environ. **29,** 6, (2020)
12. T. Li, Z. Li, E. E. Deans, et al. Nat Microbiol. **6,** 5, (2021)
13. K. Horsfield, G. Cumming. J Appl Physiol. **24**, 3 (1968)
14. E. R. Weibel. Morphometry of the human lung. (1963)
15. S. Miyawaki, S. Choi, E. A. Hoffman, C. L. Lin. J Comput Phys. **326**, (2016)
16. O. J. Ilegbusi, Z. Li, B. Seyfi, et al. Int J Biomed Imaging. (2012)
17. S. A. Nadeem, E. A. Hoffman, P. K. Saha. Conference on Medical Imaging: Image Processing. (2019)
18. D. Jin. digital topologic and geometric approaches for ct-based multi-generation characterization of airway and pulmonary vascular tree morphology and their association. (2016)
19. O. Parkash. Respiration. **34**, (1977)
20. Y. Kudo, H. Saji, Y. Shimada, et al. Eur J Cardio-Thorac. **42**, 3, (2012)
21. A. E. Sahmoun, L. D. Case, T. J. Santoro, G. G. Schwartz. Anticancer Res. **25,** (2005)
22. R. Winkler-Heil, M. Hussain, W. Hofmann. Inhal Toxicol. **33**, 3, (2021)
23. P. Koullapis, S. C. Kassinos, J. Muela, et al. Eur J Pharm Sci. **113**, (2018)
24. L. J. Calder, S. Wasilewski, J. A. Berriman, P. B. Rosenthal. P Natl Acad Sci USA. **107,** 23, (2010);
25. A. Harris, G. Cardone, D. C. Winkler, et al. P Natl Acad Sci USA. **103,** 50, (2006)
26. B. Mondeja, O. Valdes, S. Resik, et al. J Virol. **18**, 1, (2021)
27. C. G. Golding, L. L. Lamboo, D. R. Beniac, T.F. Booth. Sci Rep-Uk. **6**, (2016)
28. P. G. Koullapisa, L. Nicolaoub, S. C. Kassinos. Aerosol Sci Tech, **117**, (2018)
29. F. Lizal, M. Belka, J. Adam, J. Jedelsky, M. Jicha. P I Mech Eng H. **229**, 10, (2015)
30. T. Chan, M. Lippmann. Am Ind Hyg Assoc J. **41**, 6, (1980)
31. Y. Zhou, Y. S. Cheng. Aerosol Sci Tech, **39**, 6, (2005)